

Table 2. Ninningerite: Metal:sulfur ratios (atomic proportions), and formulas on the basis of one sulfur.

Meteorite, No.	Metal:sulfur	Formula
Abee, 1	0.991	(Fe <sub>0.52</sub> Mg <sub>0.33</sub> Mn <sub>0.06</sub> Ca <sub>0.06</sub> Cr <sub>0.03</sub> Zn <sub>0.004</sub> )S
Saint Sauveur, 2	1.010	(Fe <sub>0.47</sub> Mg <sub>0.40</sub> Mn <sub>0.05</sub> Ca <sub>0.05</sub> Cr <sub>0.03</sub> )S
Adhi-Kot, 3	0.973	(Fe <sub>0.47</sub> Mg <sub>0.36</sub> Mn <sub>0.10</sub> Ca <sub>0.04</sub> Cr <sub>0.03</sub> )S
Indarch, 4	1.047	(Fe <sub>0.31</sub> Mg <sub>0.57</sub> Mn <sub>0.05</sub> Ca <sub>0.02</sub> Cr <sub>0.02</sub> )S
St. Mark's, 5	0.993	(Fe <sub>0.20</sub> Mg <sub>0.04</sub> Mn <sub>0.15</sub> Ca <sub>0.009</sub> Cr <sub>0.002</sub> )S
Kota-Kota, 6	1.005	(Fe <sub>0.19</sub> Mg <sub>0.66</sub> Mn <sub>0.14</sub> Ca <sub>0.007</sub> Cr <sub>0.002</sub> )S

± 1 percent; accuracy, ± 3 to 5 percent of the amount present, depending on the element and its concentration. Because of such high precision, we considered it worthwhile for comparative purposes to report the data to three significant figures, even though the accuracy may not be better than ± 5 percent.

Table 1 lists averages and ranges in the composition of niningerite in each meteorite in order of decreasing iron content. Obviously, composition varies appreciably between meteorites—from (Fe<sub>0.52</sub>Mg<sub>0.33</sub>Mn<sub>0.06</sub>Ca<sub>0.06</sub>Cr<sub>0.03</sub>Zn<sub>0.004</sub>)S in Abee to (Fe<sub>0.19</sub>Mg<sub>0.66</sub>Mn<sub>0.14</sub>Ca<sub>0.007</sub>Cr<sub>0.002</sub>)S in Kota-Kota. The elements Ca and Cr follow Fe, increasing with increase in Fe, while Mn and Mg decrease with increase in Fe. Sulfur content also decreases with increasing Fe because FeS has less S than either MnS or MgS. Furthermore, appreciable differences in composition are sometimes observed between different grains of the mineral in one meteorite (Tables 1 and 2), a situation that markedly contrasts with the homogeneity of the individual mineral grains. Variations in composition within any one grain usually do not exceed the degree of accuracy of the measurements.

Regarding x-ray diffraction, attempts to separate niningerite in the pure state, using heavy media, failed because of the intimate association of the mineral with metallic nickel-iron and troilite (Fig. 2); magnetic separation failed for the same reason. Accordingly the mineral was subjected to x-ray analysis *in situ* by use of the following procedure: The polished, niningerite-bearing, plastic-mounted samples of meteorite used for electron-microprobe analysis were clamped into the sample holder of a Philips-Norelco diffractometer in such a way that the polished surfaces of the meteorites intercepted the x-rays as would smears on glass slides. Finely

ground silicon, sprinkled on the surfaces of the meteorites, served as the "internal" standard, and chart and scanning speeds were set, respectively, at 5 cm/min and ¼° 2θ/min.

Within the 28° to 51° 2θ range, the two most intense reflections corresponding to niningerite were weakly developed but distinguishable from peaks due to other minerals: their *d*-spacings (Abee niningerite), together with indices based on assumption of similarity in structure to alabandite, are 2.584 Å (200) and 1.829 Å (220) (11). Cell edges, calculated from these reflections, are listed in Table 1; because only the two peaks were available, the lattice parameters are considered no more accurate than ± 0.02 Å. The values do not vary within the assigned range of error of determination, and the average value (5.17 Å) is just less than the cell edge of alabandite (5.22 Å). Calculated densities show an appreciable range, however, because, depending on the extent to which lighter magnesium and heavier iron cations have taken each other's

place in the structure, the molecular weights of the six examples of niningerite vary considerably.

The possible origin of this mineral and the complex mineral assemblage present in enstatite chondrites are discussed elsewhere (1).

KLAUS KEIL

K. G. SNETSINGER

Space Sciences Division, National Aeronautics and Space Administration, Ames Research Center, Moffett Field, California

#### References and Notes

1. K. Keil, *J. Geophys. Res.*, in press.
2. Ferroan alabandite was also described by Keil and Andersen [*Geochim. Cosmochim. Acta* 29, 621 (1965)] from the type-II enstatite chondrite Jajh deh Kot Lalu (Fig. 1, point 7). A somewhat more Mg-rich compound was discovered by Keil and Fredriksson [*Geochim. Cosmochim. Acta* 27, 939 (1963)] in the Norton County enstatite achondrite and was properly named ferromagnesian alabandite (Fig. 1, point 16).
3. The proposed name honors H. H. Ninninger, Sedona, Arizona, for his outstanding contributions to meteoritics; name and definition have been approved by the Commission on New Minerals and Mineral Names, Intern. Mineral. Assoc. Ninningerite was first described before the 29th Annual Meeting of the Meteoritical Society, 3-5 Nov. 1966, Washington, D.C.
4. K. R. Dawson, J. A. Maxwell, D. E. Parsons, *Geochim. Cosmochim. Acta* 21, 127 (1960).
5. P. Ramdohr, *J. Geophys. Res.* 68, 2011 (1963).
6. E. R. Du Fresne and E. Anders, *Geochim. Cosmochim. Acta* 26, 251 (1962).
7. We thank E. Anders and E. R. Du Fresne for providing their original samples.
8. We thank G. Goles for these samples.
9. I. A. Yudin and S. I. Smishlaev, *Meteoritika* 25, 96 (1964).
10. K. Fredriksson and F. E. Wickman, *Särtryck ur Svensk Naturvetenskap* (1963), p. 121.
11. Two meteorites, Kota-Kota and Adhi-Kot, contain niningerite in such small amounts that no peaks corresponding to the mineral were noted.
12. We thank B. Mason and C. B. Moore for providing the samples, J. Erlichman for assistance with the electron-microprobe work, and Sally Craig for the microphotograph of niningerite.

28 October 1966

## Digital Model of Evaporite Sedimentation

Abstract. *A deterministic digital model to simulate evaporite sedimentation permits experimentation with depth of water, shape of salt basin, number, position, and strength of the inlets, and rate of evaporation. It provides a reasonable fit to salt thickness and distribution in the Upper Silurian Salina Formation of Michigan.*

Evaporite rocks, salts of the more soluble ions in seawater, are deposited when seawater becomes concentrated by excess evaporation in marginal basins having restricted circulation with the open sea. The simple conceptual model of an evaporite basin (Fig. 1) has a bar or reef near the mouth of its single inlet which restricts circulation with the sea.

As the oceanic water flows from the inlet into the basin it tends to form

a thin layer of brine that spreads over the surface of the basinal brine, and, as it does, the salt concentration in the surface layer gradually increases because of the continued evaporation of the water. When the solubility products of the salts in the surface layer are exceeded, the salts precipitate and settle to the bottom of the basin. The order of precipitation of the salts follows the order of least solubility. Normally the carbonates separate first,

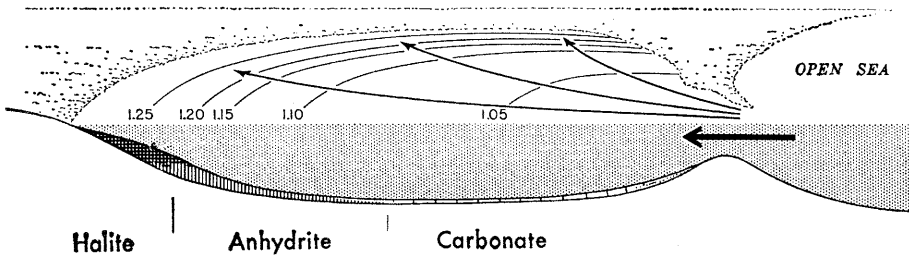


Fig. 1. A simplified model of an evaporite basin, having a single inlet connecting the basin with the open ocean.

followed by the sulfates and chlorides and the more complex double salts. In nature there is considerable overlap in their ranges of precipitation. The flow of water in the basin (Fig. 1) diverges from the inlet essentially perpendicular to the lines of equal salinity in the surface brine. The distribution of salts deposited in such a model will parallel the isosalinity lines, being arcuate and concave toward the inlet (1).

The circulation in such a basin can be determined by solving the differen-

tial equations of motion of a fluid, subject to appropriate boundary conditions at the margins of the basin. The motivation of the basin circulation is the influx of normal ocean brine, drawn into the basin as replenishment for water lost by evaporation. For simplicity in determining the circulation we have assumed: (i) steady, horizontal, irrotational flow, (ii) inviscid incompressible fluid, (iii) changes in brine density do not modify the circulation significantly, (iv) constant rate of evaporation, which acts as a distributed

surface sink, and (v) a basin of uniform depth. With these assumptions, the flow can be described by the equations:

$$-\text{div}(\rho \mathbf{v}) = \rho E/h \quad (1)$$

$$\rho = \text{constant} \quad (2)$$

$$\mathbf{v} = -\text{grad } \Phi \quad (3)$$

where  $\mathbf{v}$  is the brine velocity vector,  $\rho$  the density,  $E$  the rate of evaporation,  $h$  the depth of the basin, and  $\Phi$  a velocity potential function. By substitution in Eq. 1 we obtain:

$$\text{div grad } \Phi = E/h \quad (4)$$

a Poisson equation for the velocity potential.

The specification of the flux normal to the boundary of the entire basin renders the system determinate. At a shoreline the flux is zero; at an inlet or outlet it takes on positive or negative values respectively. The numerical solution for the velocity potential was achieved by the Gauss-Seidel point iterative method on a high-speed digital computer (2). Computed flow vectors for the simple model of Fig. 1 are shown in Fig. 2a.

The transport, progressive concentration, and eventual precipitation of a chemical component dissolved in the fluid can be obtained by solving

$$-\text{div}(-\delta \text{grad } C + C\mathbf{v}) = \partial C/\partial t \quad (5)$$

where  $C$  is the concentration field measured in mass of dissolved component per unit volume of brine,  $\mathbf{v}$  is the velocity field determined from  $\mathbf{v} = -\text{grad } \Phi$ ,  $\delta$  a diffusion constant, and  $t$  is time. The diffusive transport is included for completeness, but in other than static systems, its magnitude is ordinarily negligible. The initial condition for the concentration field is the concentration of normal ocean brine.

The numerical solution of Eq. 5 yields a sequence of "snapshots" of the concentration field at successively later times after the onset of evaporation (Fig. 2, b-d). The time scale of the process is dominated by the rate of evaporation, which can be estimated from present day evaporite basins. When the brine becomes sufficiently concentrated, precipitation will occur. Precipitation is calculated by removing from the brine any dissolved mass which enters a zone which has already reached a prescribed "saturation" concentration. The excess mass so removed is converted to an equivalent thickness of precipitate per unit area

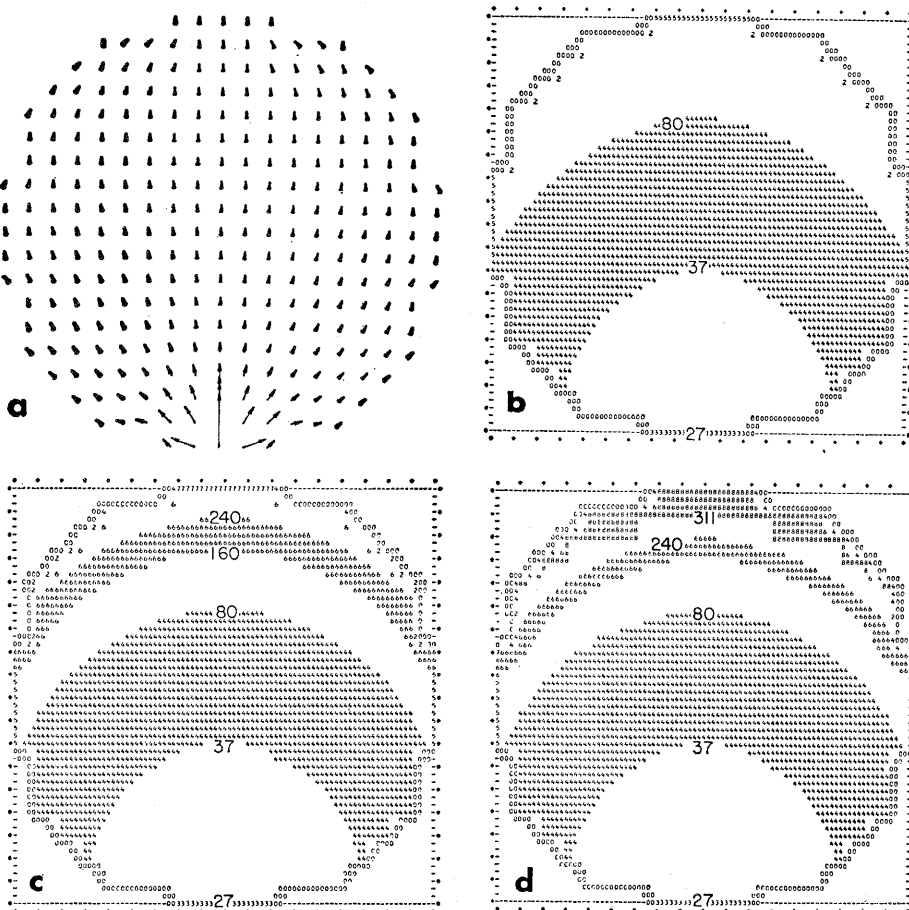


Fig. 2. Results of model computations. (a) Computed velocity vectors for a simple circular evaporite basin with replenishment from a single inlet. (b-d) Distribution of brine concentrations after 500, 1000, and 1500 years, respectively. Values shown are in grams of NaCl per liter of brine. In the 1500 year pattern, saturation (311) has been reached at the distal end of basin, and deposition is underway.

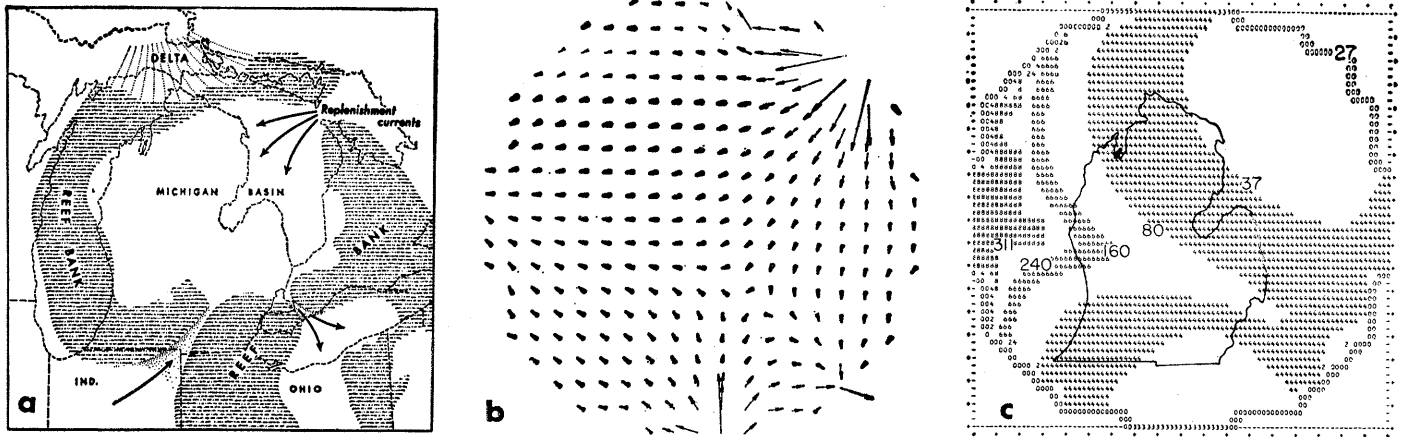


Fig. 3. Stratigraphic model and results of computations. (a) Cayugan paleogeography, showing reef banks ringing the basin, with prominent replenishment currents and one small outlet also indicated. (b) Computed velocity vectors from numerical model of (a). (c) Concentration pattern after 1500 years in model with velocity distribution shown in (b). Zone of saturation and deposition are west of basin center.

of the basin floor, and demobilized at that point on the floor as an evaporite deposit. In these initial experiments we considered only a single component system, a simplified normal ocean brine consisting of 27 g of dissolved NaCl per liter of solution. Precipitation in this system will occur at concentrations greater than 311 g of NaCl per liter of brine.

The flexibility of this method of deterministic modeling is sufficient to permit experimentation with the depth and shape of the basin, the number, the position and size of inlets from the open ocean, and the rate of evaporation. An experiment consists of designating these factors, computing the resulting circulation in the basin, and monitoring the brine concentration at a network of points as evaporation contin-

ues with time. Saturation and deposition eventually occur, and the location, thickness, and time of deposition can be observed.

The simplified model of evaporite rock deposition can be tested for its validity against ancient evaporite deposits. The Upper Silurian Salina Formation of the Michigan Basin is one of the better known evaporite deposits (3). Extensive stratigraphic studies have suggested that during the Late Silurian period the Michigan Basin was ringed by a widespread platform reef bank which draped over the shoulders of the bordering Findlay-Algonquin and Kankakee structural arches and the Canadian Shield (Fig. 3a). Two principal inlets fed oceanic brine into the central evaporite basin from the northeast and south, whereas some

basinal brine seems to have flowed through the Chatham Sag across the Findlay-Algonquin Arch into the Ohio portion of the Appalachian Basin on the southeast. Other less prominent inlets or passes through the reef platform may have existed, but they are individually too small to affect the nature and distribution of the evaporite deposits on the scale studied.

The thickness and distribution of halite deposited in the Michigan Basin during the Late Silurian period (Fig. 4c) will be used as a test of the numerical model. The velocity vector field for the two major inlets and one minor outlet modeled after the Salina salt basin (Fig. 3b) produced a precipitation pattern (Fig. 3c) too far west of that observed in the Salina salt deposition. No amount of modification

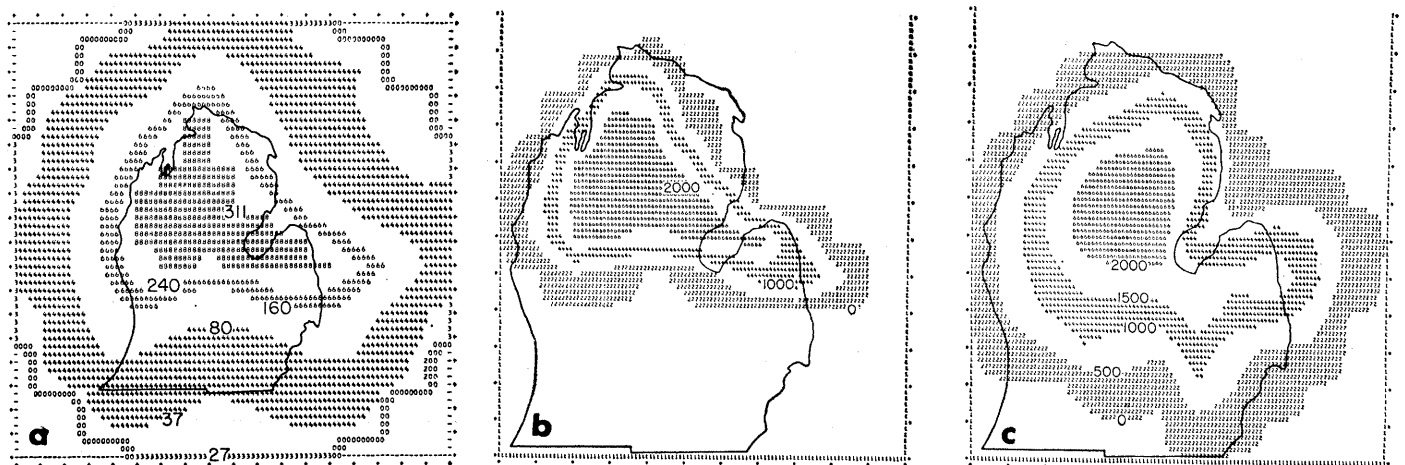


Fig. 4. Modified stratigraphic model and its comparison with geologic data. (a) Concentration pattern after 1500 years in model which has 80 percent of replenishment via radial inflow through "leaky" reefs, 20 percent via major open inlets. Deposition occurs in center of basin. (b) Thickness in feet of deposits in saturated zone of (a) after 12,000 years. (c) Isopach map of these deposits is the "goal" of the simulation.

of the relative flow volumes through the two inlets and one outlet could move the major salt deposition to the central part of the basin.

A much more successful model incorporated radial influx around the entire periphery of the basin in addition to the two inlet and one outlet flow. This is analogous to a "leaky" peripheral reef bank through which there are several water passages. The structure is similar to that of many atolls. The resulting salt concentration pattern (Fig. 4a) and salt thickness distribution (Fig. 4b) more realistically simulate the Salina salt deposition.

In addition, the rates of concentration and precipitation of salt compare favorably with those adduced for natural deposits (4). The first precipitation occurs in the simulation model about 1000 years after evaporation becomes dominant. A steady state in the brine concentration pattern and rate of salt precipitation occurs at about 2000 years. Approximately 12,000 years are needed to build up the 750 m of salt in the center of the basin. The critical factor that determines rate of concentration and precipitation is the net rate of evaporation, which for our experiments was chosen at 50 cm per year. In comparison with evaporite basins today, the rate is conservative.

We do not infer that the 750 m of salt in the Salina Formation was deposited in 12,000 years; only that it could have been deposited in a very short period of time if the optimum conditions for salt precipitation per-

sisted. The Salina rocks are not only salt, but a complex sequence of evaporite and normal marine sediments which involved a longer and more complex history.

The simplified deterministic model of evaporite rock deposition, based on steady, horizontal, irrotational flow of idealized seawater into the evaporite basin, can be made to approximate the observations of the salt distribution pattern of a real geological situation. The rapidity of deposition inferred from the model is substantiated by chemical and geological data.

One lesson that might be drawn from this model and the associated experiments is that very simple geological processes combined in the proper manner can closely simulate nature. When sufficient knowledge exists concerning the processes and the geology, there is no need to invoke random, probabilistic processes.

L. I. BRIGGS

H. N. POLLACK

*Department of Geology and Mineralogy, University of Michigan, Ann Arbor*

#### References and Notes

1. L. I. Briggs, *J. Sediment. Petrol.* **28**, 46 (1958).
2. D. M. Young, in *Survey of Numerical Analysis*, J. Todd, Ed. (McGraw-Hill, New York, 1962), p. 380.
3. H. L. Alling and L. I. Briggs, *Bull. Amer. Assoc. Petrol. Geol.* **45**, 515 (1961).
4. R. H. King, *ibid.* **31**, 470 (1947); W. B. Lang, *Bull. Geol. Soc. Amer.* **61**, 1479 (1950); L. I. Briggs, *Michigan Acad. Sci. Papers 1956* **42**, 115 (1957); Y. K. Bendor, *Geochim. Cosmochim. Acta* **25**, 239 (1961).
5. Research supported by NSF grant GP-3833.

8 November 1966

## Trial Balloons in the Southern Hemisphere

**Abstract.** *Superpressure GHOST balloons are being launched from Christchurch, New Zealand, to determine their life, stability, and clustering characteristics at several altitudes. Three separate balloons have flown for more than 6 months at 200 millibars, proving capability of the long life that had been hoped for at such middle altitudes and providing preliminary trajectory data for the Southern Hemisphere. Icing problems at lower altitudes have not yet been solved. We expect future flight durations of several years at higher altitudes. If successful, the new balloons will be useful platforms for experimenters concerned with study of large-scale and long-term effects in the stratosphere.*

An extensible helium- or hydrogen-filled balloon of rubber or neoprene, which ascends, expands, and bursts, is the vehicle normally used by meteorologists to obtain atmospheric data. The highest known altitude reached by a neoprene balloon is 47.5 km.

The unextensible balloon, usually of rubberized fabric for manned ascents

and polyethylene film for carrying instruments, is partially inflated on the ground. As it ascends, its gas content expands to fill the envelope, which must have a vent to release excess gas and so prevent rupture. Typical sporting balloons to carry people are 10 to 20 m in diameter. Balloons for transporting instruments to high altitudes

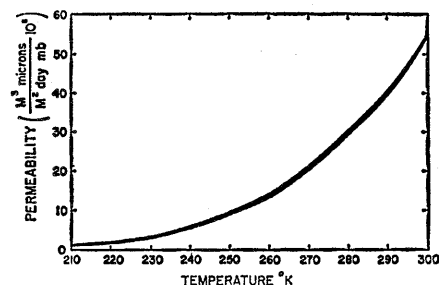


Fig. 1. Permeability of polyester film to helium.

range from 20 to 150 m in diameter. The highest known altitude reached by an unextensible balloon is 47 km; the heaviest gross load carried to date is 7000 kg (*Stratoscope II*). Ballast must be released from an unextensible balloon whenever the gas cools, if the balloon is to stay aloft; at least 5 percent of the weight of the system must be jettisoned to maintain altitude through sunset. Flights have lasted as long as 2 weeks, requiring hundreds of kilograms of ballast.

A superpressure balloon is an unextensible balloon that is not vented. When the balloon's volume is filled and it continues to ascend, the free lift is converted to overpressure; if the balloon's skin is strong enough, it will not burst. If the modulus of elasticity of the balloon's skin is high enough, its volume will increase only slightly and it will float at an altitude of constant atmospheric density. Films of polyethylene terephthalate (polyester) or cellophane are materials strong enough and having a high-enough modulus to permit stable flight; by happy coincidence, both have excellent low-diffusion characteristics for helium.

The percentage of gas lost per day through the skin of a spherical balloon may be expressed:

$$\text{Gas loss (\%)} = (300 \cdot \delta \cdot p) / (r \cdot t)$$

where  $r$  is the radius of the balloon in meters,  $\delta$  is the diffusion constant in ( $M^3$  microns)/( $M^2$  day mb),  $t$  is film thickness in microns, and  $p$  is pressure in millibars. The diffusion constant for helium as a function of temperature, for polyester film, is shown in Fig. 1; Table 1, based on such considerations, lists data on the theoretical life of balloons now being flown from Christchurch, New Zealand.

All plastics have defects. A balloon having several square meters of surface area of plastic film will inevitably have some small holes. However, if a lami-